ACS OMEGA

http://pubs.acs.org/journal/acsodf

Article

Reducing the Energy Band Gap of Cobalt Hydroxide Nanosheets with Silver Atoms and Enhancing Their Electrical Conductivity with Silver Nanoparticles

Montakan Suksomboon, Ketsuda Kongsawatvoragul, Salatan Duangdangchote, and Montree Sawangphruk*

Cite This: *ACS Omega* 2021, 6, 20804−20811

Read Online

ACCESS | Metrics & More | Article Recommendations | Supporting Information

ABSTRACT: Although cobalt hydroxide ($Co(OH)_2$) has been attracting attention in several applications, its photoelectrochemical property has not yet been fully investigated. In this work, tuning the energy band gap of $Co(OH)_2$ nanosheets with silver atoms and enhancing their electrical conductivity with silver nanoparticles were then focused. A Ag-doped α-$Co(OH)_2$ thin film was successfully synthesized *via* an electrodeposition method. The optical properties of the as-prepared materials were characterized by UV−vis and fluorescence lifetime spectroscopies and further confirmed by density functional theoretical calculation. It was found that Ag atoms between adjacent layers of $Co(OH)_2$ can reduce its electronic band gap to 2.45 eV (α-$Co(OH)_2$) as compared to 2.85 eV of β-$Co(OH)_2$. In terms of electrochemical properties, silver nanoparticles (AgNPs) can enhance the electrical conductivity of $Co(OH)_2$ nanosheets, leading to faster charge transfer reducing the internal resistance and significantly increasing the overall charge storage performance. Interestingly, under light illumination, Ag-doped α-$Co(OH)_2$ exhibits *ca.* 0.8 times lower charge storage capacity as compared to that under the dark condition. This is because the photoelectrons can be recombined with the generated holes in the conduction band. The charge storage mechanisms of Ag-doped α-$Co(OH)_2$ operated under dark conditions and light irradiation were further studied and confirmed using *in situ* electrochemical X-ray absorption spectroscopy (XAS). Overall, the *in situ* XAS supports the electrochemical result. This finding may pave a way to further develop photoactive advanced functional materials of metal hydroxides and oxides.

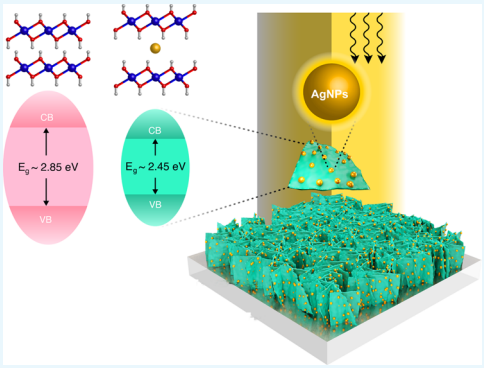

INTRODUCTION

Cobalt hydroxide ($Co(OH)_2$) with a layer structure has been well known as a promising electrode material for various energy storage and conversion applications, due to its high theoretical specific capacitance of *ca.* 3400 F g^{-1}.[1] Its nanostructure also provides a high specific surface area, allowing a large amount of electrolyte ions to be adsorbed on its surface, leading to surface redox reactions. In general, $Co(H)_2$ has two phases, namely, α and β. The difference of these two phases is the interlayer spacing between two adjacent cobalt-based layers. The α-$Co(OH)_2$ has a larger d-spacing of *ca.* 7.0 Å due to the existing solvated anions (Cl^-, Co_3^{2-}, or NO_3^-) between the positive layers, while the β-$Co(OH)_2$, which has a *d*-spacing of 4.6 Å, has no solvated anions between its adjacent layers.[2−8]

Recently, cobalt hydroxide/oxide nanostructures have been used as photoactive materials which can convert the photon energy into the electrical energy *via* the photovoltaic effect.[3,9−15] The photon energy under light illumination can provoke cobalt hydroxides to generate the charge carriers, excited electrons (e^-) and holes (h^+) in the valence band (VB) and conduction band (CB), respectively. This process can generate the extra photocurrent, leading to higher performance when $Co(OH)_2$ is served as the photoelectrode. However, their intrinsic electronic and electrical conductivities are very poor due to the nature of metal oxides and hydroxides.[16−18] Introducing highly conductive AgNPs to cobalt hydroxides can be a solution overcoming these issues by reducing their internal resistances, leading to fast charge transfer or high charge storage capacity.[19] Besides, according to the recent finding of a photocharging property of $Co(OH)_2$, its photoelectrochemical property relating to its energy band gap has not yet been fully studied.

In this work, we therefore aim to improve the electronic and electrochemical properties of $Co(OH)_2$ by the incorporation of silver atoms and silver nanoparticles (AgNPs). The

Received: April 9, 2021
Accepted: June 30, 2021
Published: August 6, 2021

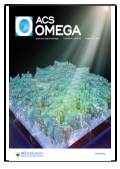

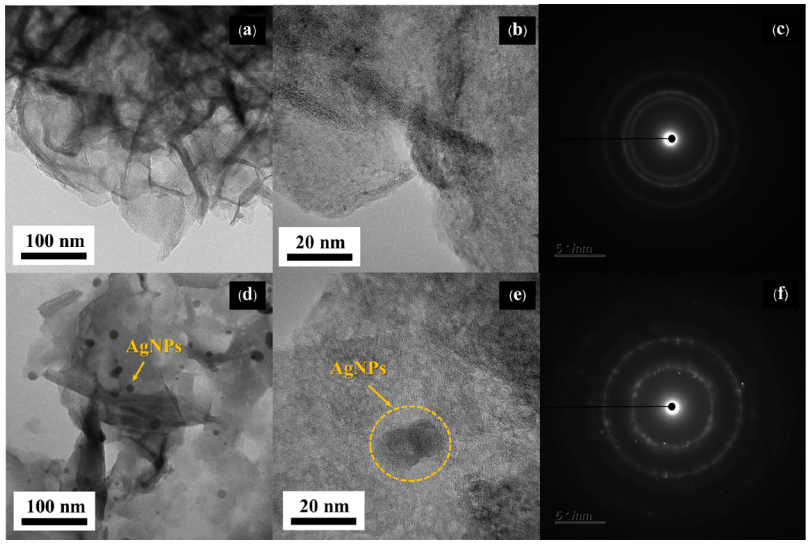

Figure 1. (a) Low- and (b) high-resolution TEM (HR-TEM) images and (c) SAED pattern of β-$Co(OH)_2$ nanosheets and (d) TEM and (e) HR-TEM images and (f) SAED pattern of Ag-doped α-$Co(OH)_2$ with AgNPs.

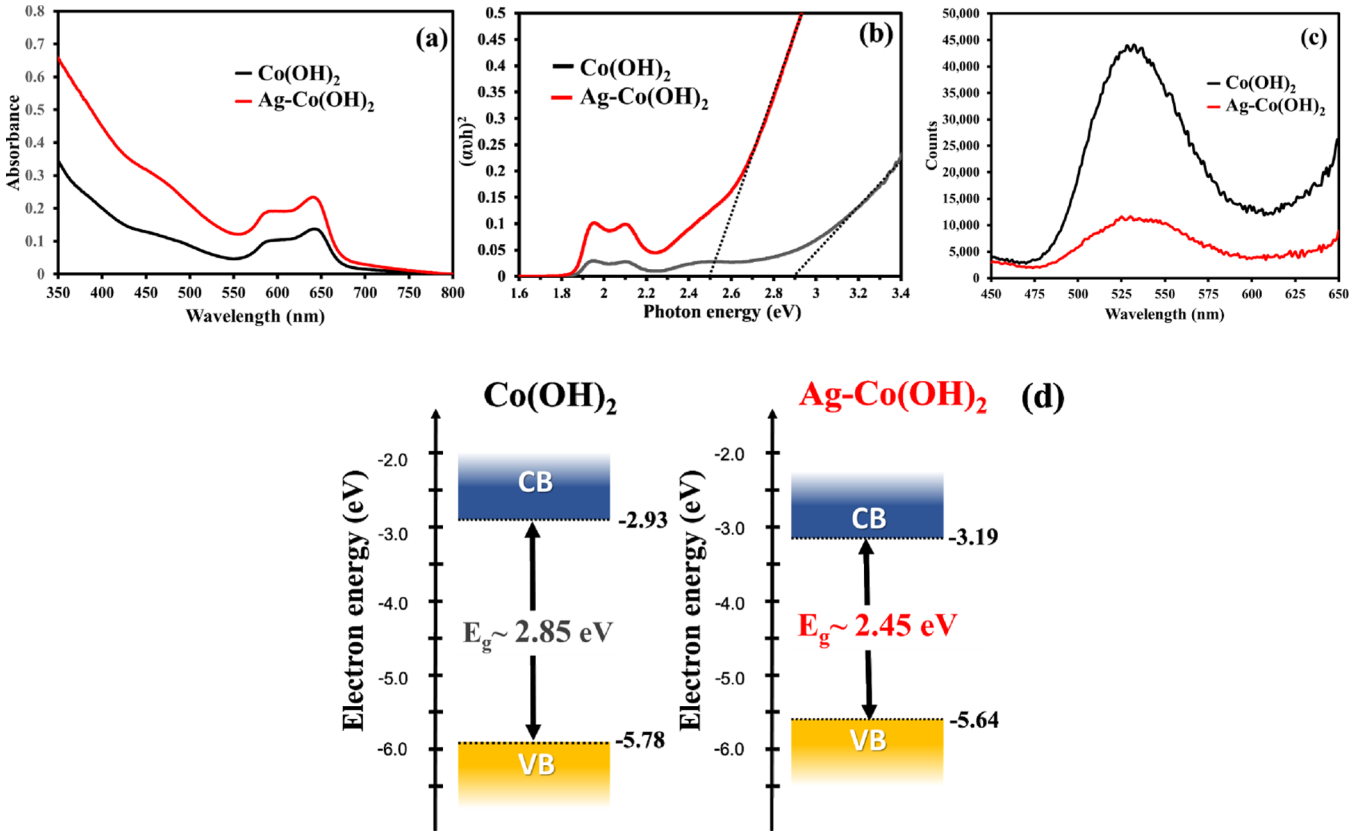

Figure 2. (a) UV−visible spectra, (b) Tauc plots, (c) fluorescence spectrum, and (d) schematic energy−level diagram of the β-$Co(OH)_2$ and Ag-doped α-$Co(OH)_2$ with AgNP photoelectrodes.

theoretical calculation along with the experiment was used to investigate the change in optical and structural properties. It was found that the Ag atom-doped α-$Co(OH)_2$ has a much lower energy band gap (2.45 eV) as compared to 2.85 eV of β-$Co(OH)_2$. At the same time, AgNPs can significantly enhance the electrical conductivity of the electrode, providing the enhancement of the charge storage capacity of the materials. Interestingly, the photoelectrode of Ag-doped α-$Co(OH)_2$ exhibits lower charge storage performance under the light irradiation compared to that under the dark condition due to the recombination of photogenerated electrons and holes in the CB. Their charge storage mechanisms were further studied by *in situ* electrochemical X-ray absorption spectroscopy (XAS).

RESULTS AND DISCUSSION

For the experiment and characterization, the silver materials were introduced to $Co(OH)_2$ nanosheets by the electro-

https://doi.org/10.1021/acsomega.1c01908
ACS Omega 2021, 6, 20804−20811

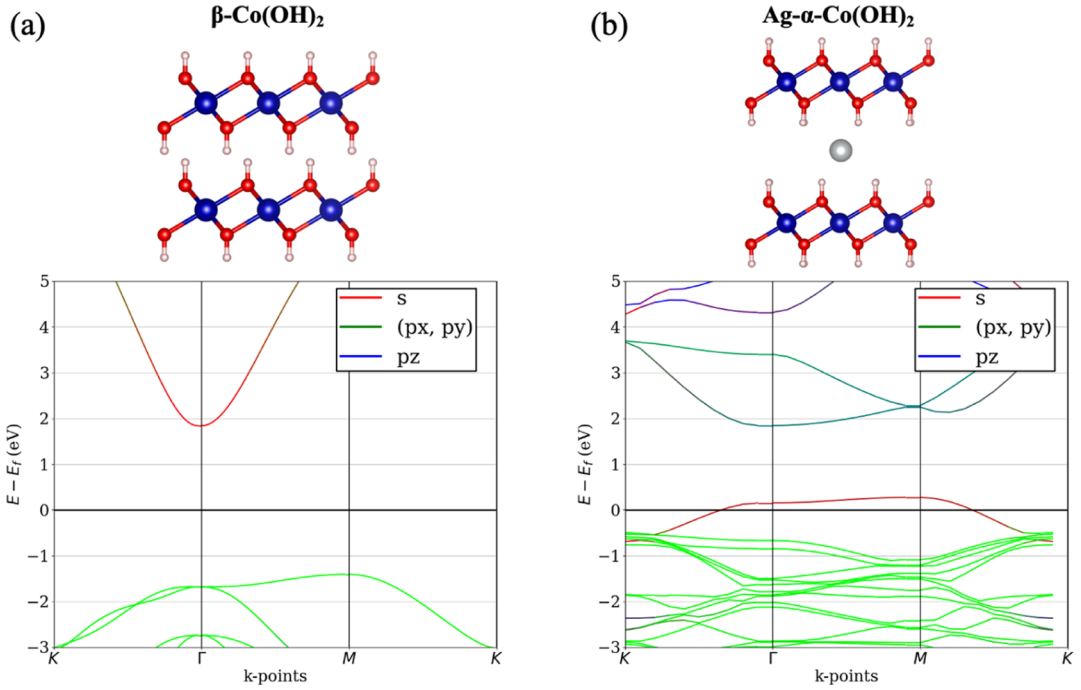

Figure 3. Optimized structures and theoretical electronic band structures of (a) β-$Co(OH)_2$ and (b) Ag-doped α-$Co(OH)_2$.

deposition method using a transparent conductive fluorine-doped tin oxide (FTO) glass as a working electrode (WE) (see more details in the Experimental Section). The surface and cross-sectional morphologies of the as-electrodeposited materials were characterized by field-emission scanning electron microscopy (FE-SEM). As seen from the low-magnification FE-SEM images of both $Co(OH)_2$ and Ag-doped $Co(OH)_2$ electrodes in Figure S2a,b, the nanosheets of $Co(OH)_2$ arrays are vertically and uniformly standing on the FTO surface. High-magnification FE-SEM images (Figure S2c,d) illustrate the $Co(OH)_2$ nanosheets with an interconnected network forming high porosity. The average thickness of a stacked-sheet $Co(OH)_2$ is *ca.* 45 nm, while Ag-doped $Co(OH)_2$ has a thinner sheet with a thickness of *ca.* 25 nm with AgNPs decorated on the sheets. The cross-sectional FE-SEM images of $Co(OH)_2$ and Ag−$Co(OH)_2$ are shown in Figure S3 with a film thickness of *ca.* 950 and 480 nm, respectively. Transmission electron microscopy (TEM) images of $Co(OH)_2$ shown in Figure 1a,b illustrate the sheet-like structure of β-$Co(OH)_2$ with a *d*-spacing of ca. 4.6 Å. For Ag−$Co(OH)_2$, the AgNPs with an average diameter of *ca.*10 nm are clearly observed on the $Co(OH)_2$ nanosheets (Figure 1d,e). In addition, by focusing the crystalline region of $Co(OH)_2$, the α-phase with a d-spacing of *ca.* 7.0 Å is observed. Furthermore, the corresponding selected-area electron diffraction (SAED) pattern of Ag−$Co(OH)_2$ (see Figure 1f) depicts a higher polycrystalline structure after being doped with AgNPs compared to that of β-$Co(OH)_2$ (see Figure 1c). This suggests that the β-$Co(OH)_2$ structure is transformed to be an amorphous phase of Ag-doped α-$Co(OH)_2$ with 10 nm AgNPs.[19] The structures of $Co(OH)_2$ and Ag-doped $Co(OH)_2$ were also characterized by X-ray diffraction (XRD), as shown in Figure S6. The XRD patterns are in good agreement with the TEM results. The introduction of Ag to $Co(OH)_2$ can provide an amorphous phase of α-$Co(OH)_2$.

To understand the optical properties of the β-$Co(OH)_2$ and Ag-doped α-$Co(OH)_2$ with AgNPs, UV−visible spectroscopy was utilized. Figure 2a depicts the light absorbance spectra of the β-$Co(OH)_2$ and Ag-doped α-$Co(OH)_2$ with AgNPs in the absorption band range of 350−800 nm. Two obvious peaks observed on both electrodes in a range of 560−680 nm correspond to the tetrahedral coordination of Co^{2+} in $Co(OH)_2$[2]. In addition, the main absorption of both samples at *ca.* 400 nm was used to determine their optical band gaps based on the Tauc equation. The addition of Ag to $Co(OH)_2$ nanosheets can affect the energy band gap of $Co(OH)_2$ due to the formation of Ag atom-doped α-$Co(OH)_2$. This has been confirmed by the density functional theory (DFT) calculation (see Figure 3). The energy band gaps can be extrapolated to be 2.85 and 2.45 eV for the β-$Co(OH)_2$ and Ag-doped α-$Co(OH)_2$ with AgNPs, respectively. The optical band gap of Ag−$Co(OH)_2$ is narrower than that of β-$Co(OH)_2$ due to the intrinsic property of the α-phase of $Co(OH)_2$. A fluorescence lifetime spectrometer was also utilized to investigate the electron excitation of the as-synthesized photoelectrodes. Figure 2c illustrates the fluorescence lifetime spectroscopy (FLS) results of the β-$Co(OH)_2$ and Ag-doped α-$Co(OH)_2$ with AgNPs. The peaks of both electrodes are located at the same position, but the signal of the Ag-doped α-$Co(OH)_2$ electrode is lower than that of β-$Co(OH)_2$ when excited at the same wavelength (430 nm). This result suggests that both electrodes can generate the electron−hole pair by photo-excitation. However, the Ag-doped α-$Co(OH)_2$ with AgNPs demonstrates a lower intensity of the broad absorption band centered at *ca.* 520 nm, which is a characteristic of the octahedral coordination of cobalt in α-$Co(OH)_2$. This is in good agreement with XRD and Fourier transform infrared results in the previous work.[19] In addition, a lower intensity of fluorescence emission indicates a lower photoelectron excitation. Furthermore, a photoelectron spectrometer was used to determine the VB and edge of the as-prepared electrodes by measuring their ionization energies. The results

https://doi.org/10.1021/acsomega.1c01908
ACS Omega 2021, 6, 20804−20811

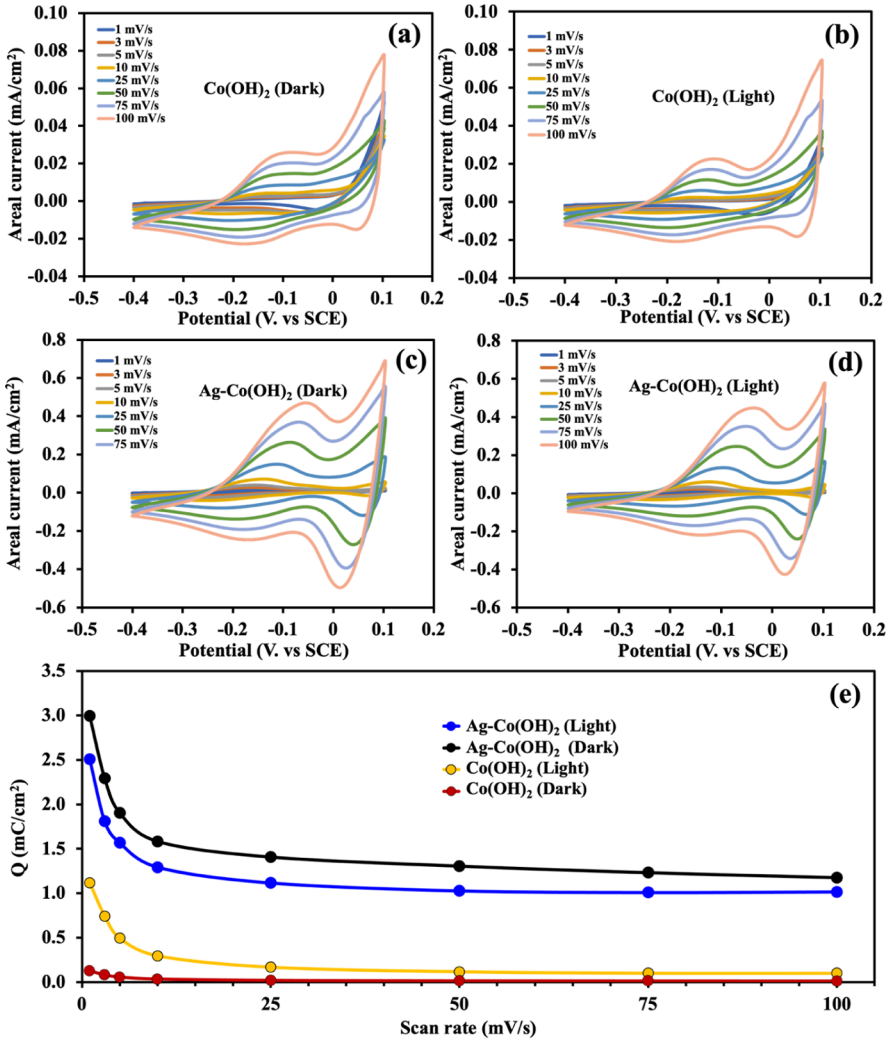

Figure 4. Cyclic voltammograms of β-$Co(OH)_2$ under (a) dark and (b) light illumination and Ag-doped α-$Co(OH)_2$ with AgNPs under (c) dark and (d) light illumination. The electrodes were tested in 1 M NaOH at different scan rates. (e) Areal stored charge of β-$Co(OH)_2$ and Ag-doped α-$Co(OH)_2$ with AgNPs under dark and light conditions.

show that the β-$Co(OH)_2$ and Ag-doped α-$Co(OH)_2$ with AgNPs have VB edges of 5.78 and 5.64 eV, respectively. The schematics of the energy−level diagram is depicted in Figure 2d, suggesting that the silver incorporation narrows the energy band gap.

All calculations reported in this work were performed by Vienna *ab initio* simulation package (VASP)[20−22] based on the periodic plane-wave DFT. The optimized lattice constants of the bulk unit cell are obtained as c = 4.594 Å for β-$Co(OH)_2$ and c = 7.09 Å for Ag-α-$Co(OH)_2$. This is reasonably in good agreement with the experimentally obtained d-spacing values, 4.6 Å from the literature for β-$Co(OH)_2$ and 7.0 Å for ion-implanted α-$Co(OH)_2$.[2−6] The band structure calculation in Figure 3 indicates that the presence of Ag in the structure of $Co(OH)_2$ causes a significant reduction of the band gap.

To study the electrochemical property of the prepared electrodes, cyclic voltammetry (CV) was performed with a three-electrode system. All electrodes were tested in the tree-electrode system using 1 M NaOH as an aqueous electrolyte solution. The platinum rod and saturated calomel electrode (SCE) were used as a counter electrode and a reference electrode (RE), respectively. The as-fabricated electrodes were tested using CV with a potential range of −0.4 to 0.1 V versus SCE at different scan rates of 1, 2, 3, 5, 10, 25, 50, 75, and 100 mV s^{-1} (see Figure 4a−d). Under the dark condition, the Ag-doped α-$Co(OH)_2$ with AgNPs exhibits higher capacity compared to the undoped β-$Co(OH)_2$. This is due to its higher electrical conductivity, leading to faster charge transfer. However, under the light illumination, the decreasing capacity of Ag-doped α-$Co(OH)_2$ with AgNPs was observed (see Figure 4e). This is because of the too narrow band gap of Ag-doped α-$Co(OH)_2$ and plasmonic property of AgNPs, which can trap the light or photon reducing the photoelectron.[23] Under light illumination, the photoelectron generated via the photelectric effect can enhance the charge storage performance of $Co(OH)_2$, but with the incorporation of Ag in the adjacent layer and AgNPs, the competitive surface plasmon resonance process occurs in parallel on AgNP surfaces, leading to the lower charge storage performance observed in the Ag-containing system.

The change in the oxidation state of Co during the electrochemical process is crucial evidence for determining a charge mechanism investigation of electrode materials. In this work, the oxidation number of Co plays a significant role in redox reactions during charging and discharging. To gain an in-depth understanding of the local structural change in Co and

https://doi.org/10.1021/acsomega.1c01908
ACS Omega 2021, 6, 20804−20811

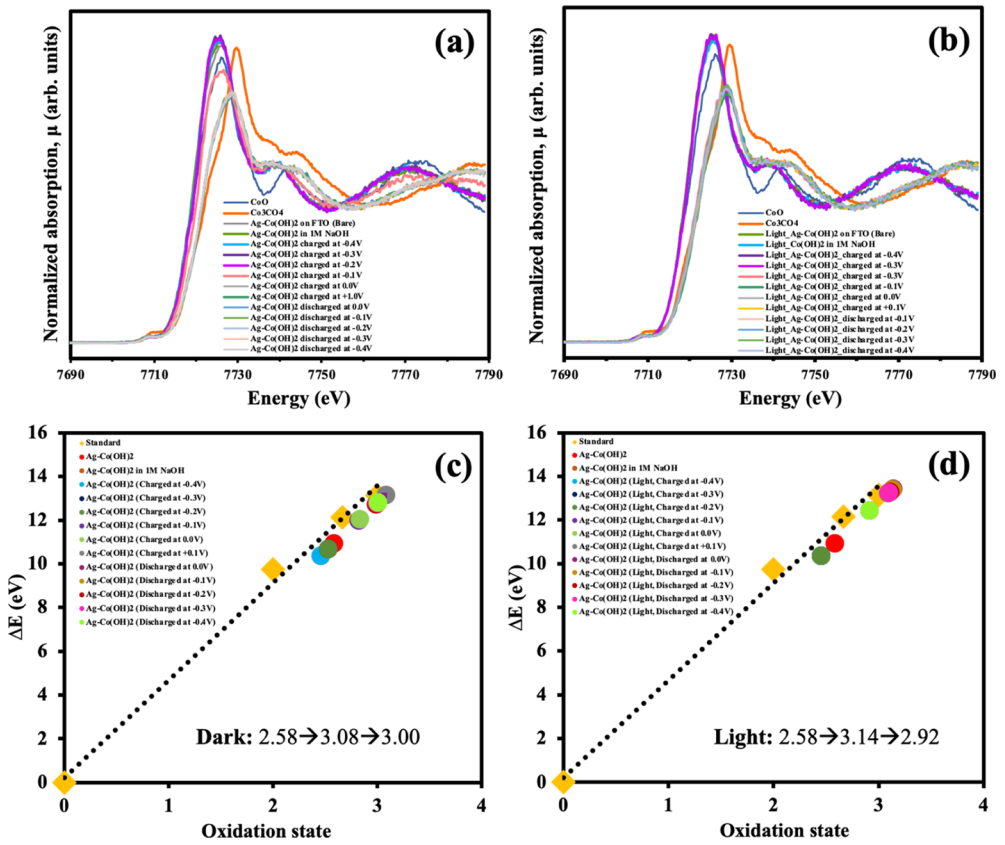

Figure 5. *In situ* high-resolution Co−K edge fluorescence XANES spectra of the Ag−$Co(OH)_2$ electrode under (a) dark and (b) light conditions, compared to other Co standard compounds. The oxidation states vs ΔE (eV) of the Ag−$Co(OH)_2$ photoelectrode during the charge/discharge processes at applied potentials (c) without light and (d) with light illumination, determined from the Co K-edge relative to the reference cobalt oxides.

their pseudocapacitive behavior when the photoelectrodes are charged and discharged, *in situ* XAS with a fluorescence mode was carried out. The absorption edge energy of both electrodes, β-$Co(OH)_2$ and Ag-doped α-$Co(OH)_2$ with AgNPs, was determined during the electrochemical measurement using chronoamperometry under dark conditions and light illumination in 1 M NaOH (See Figure S1). The design of the *in situ* electrochemical cell was reported in our previous work.[24] Before starting the X-ray absorption near-edge structure (XANES) measurement, all photoelectrodes were held for 15 min at each potential to obtain the fully charged state or the steady state. The cobalt standard compounds of Co metal foil (Co^0), CoO (Co^{2+}) and Co_2O_3 (Co^{3+}) were used as references. The normalized Co−K edge XANES spectra of Ag-doped α-$Co(OH)_2$ with the AgNP photoactive electrode under dark and light irradiation at different applied potentials (the same range of the CV experiment) are shown in Figure 5a,b, respectively. Their oxidation numbers, calculated using a linear relationship, compared with those of Co standards are plotted in Figure 5c,d. The average oxidation state of Co in the Ag−$Co(OH)_2$ is +2.58 at an energy edge of 7719.89 eV, which is between Co^{2+} and Co^{3+}. This result refers to Co^{2+}/Co^{3+} mixed valences. The initial oxidation state of Co in the Ag-doped α-$Co(OH)_2$ in 1 M NaOH is found to be +2.46 eV. By applying the potential from −0.4 to 0.1 V. versus SCE, the edge positions are significantly shifted to higher energy for both conditions, indicating an increasing oxidation state of Co during the charging process. Under the dark condition with the fully charged state of Ag-doped α-$Co(OH)_2$, the oxidation state of Co is increased to be +3.08, while that under light illumination is found to be +3.14. The higher oxidation number of the Ag−$Co(OH)_2$ electrode under light illumination for the forward scan is because of the photovoltaic effect, generating the photoelectrons. However, at the backward scan, the oxidation number of Co in the Ag−$Co(OH)_2$ under dark conditions is +3.0, while that under light irradiation decreases to +2.92. It can be summarized here that when the Ag-doped α-$Co(OH)_2$ photoelectrode is discharged, the photoelectrons can be recombined with the generated holes in the CB, while the photoexcited electrons under dark conditions transfer to the external system.

CONCLUSIONS

In summary, an incorporation of Ag to $Co(OH)_2$ does affect the photoelectrochemical performance of $Co(OH)_2$. Ag-doped α-$Co(OH)_2$ nanosheets synthesized via a simple electrodeposition method exhibit a narrower energy band gap (2.45 eV) as compared to that of β-$Co(OH)_2$ (2.85 eV), leading to higher electrical conductivity. The significant change in the optical property is due to the silver intercalated at the adjacent layers of α-$Co(OH)_2$. The energy band gap reduction and the phase transformation after doping with Ag were further confirmed by DFT calculation. The as-prepared β-$Co(OH)_2$ and Ag-doped α-$Co(OH)_2$ with AgNP photoelectrodes were also electrochemically tested by the *in situ* XAS in 1 M NaOH under dark and light illumination conditions. Under dark conditions, the Ag-doped α-$Co(OH)_2$ electrode exhibits higher capacity than the undoped one. This is because of a

https://doi.org/10.1021/acsomega.1c01908
ACS Omega 2021, 6, 20804−20811

greater electrical conductivity due to the decoration of AgNPs on the $Co(OH)_2$ nanosheets, leading to faster electron transfer. Interestingly, under light illumination, Ag-doped α-$Co(OH)_2$ with AgNPs exhibits *ca.* 0.8-fold lower charge storage performance as compared to that under the dark condition since the photoelectrons can be recombined with the generated holes in the CB. This finding may pave a way to further develop the cobalt hydroxide-based advanced functional materials for electrochemical applications.

EXPERIMENTAL SECTION

Chemicals. All reagents are of analytical grade. Cobalt (ii) nitrate hexahydrate (99%) was purchased from QRec. Sodium hydroxide (98%) was obtained from Carlo Erba. Sodium nitrate (99.0%) and silver nitrate were provided by Ajax. All solutions were made up using Milli-Q water with a resistance of 15 MΩ·cm at 25 °C. A commercial conductive FTO glass was ordered from TEC8, Dyesol Ltd., Australia.

Electrode Preparation. All electrodes in this work were prepared via the electrodeposition technique using a Metrohm AUTOLAB potentiostat (PGSTAT 302N running NOVA version 1.10.3 software). A conductive FTO glass was employed as a substrate. The precursor solution is 100mM $Co(NO_3)_2{\cdot}6H_2O$ in 0.5 M $NaNO_3$with 1 mM $AgNO_3$. For the $Co(OH)_2$ electrode, the solution is the same as above but without $AgNO_3$. The three-electrode system was set up using the FTO glass as a WE, platinum rod as a counter electrode, and Ag/AgCl (3 M KCl) as an RE. The potential of −1.0 V versus Ag/AgCl electrode was applied to the system for 5 min using a chronoamperometry method. The green film of $Co(OH)_2$ and the dark green film of Ag−$Co(H)_2$ were deposited on the substrates. Then, the electrodes were rinsed with DI water several times to remove the retained precursor before being dried at 60 °C overnight in the vacuum oven. The mass loading of the material is *ca.* 0.8 mg/cm^2.

Characterization. The morphology of the as-prepared electrodes was characterized by FE-SEM [JSM-7001F (JEOL Ltd., Japan)] and HR-TEM (JEM 1220 (JEOL Ltd., Japan)). XRD experiments were carried out using a D8 ADVANCE with DAVINCI design (Bruker optics, Germany) equipped with a Cu Kα source (l 1.5418 Å, step = 0.01°) in the 2θ range of 5−80° to study the structure of the as-prepared materials. UV−vis spectroscopy (UV/Vis/NIR Lambda 1050, PerkinElmer, USA), FLS, and photoelectron spectrometry (RIKEN, AC-2 model) were employed to investigate the optical property of all samples. The *in situ* XAS was performed to investigate the oxidation number of Co in the electrodes during charge/discharge processes.

Electrochemical Measurements. The potentiostat (PGSTAT 302N), made by Metrohm AUTOLAB, Netherlands, with NOVA version 1.10.3 software, was utilized for all electrochemical experiments. The as-prepared electrodes, $Co(OH)_2$ and Ag−$Co(OH)_2$ electrodeposited on conductive FTO glasses, served as a WE, while the SCE and Pt rod were employed as an RE and a counter electrode, respectively. 1 M NaOH was used as a basic aqueous electrolyte solution for all electrochemical measurements. CV was carried out to study the electrochemical behavior and electrochemical performance of all electrodes *via* a three-electrode setup with a potential range of −0.4 to 0.1 V versus SCE.

***In Situ* XAS.** The *in situ* XAS measurement with a fluorescence mode was carried out on the beamline no. 5.2 at the Synchrotron Light Research Institute (Public Organization), Thailand. Fluorescence Co K-edge spectra were recorded at ambient temperature using a double-crystal Ge(220) crystal. The subtraction of both pre-edge and postedge contributions and curve fitting of the normalized XANES spectra were carried out via ATHENA software. The *in situ* XAS experiment was performed along with chronoamperometry at different applied potentials in the 1 M NaOH aqueous electrolyte. The as-prepared electrode was applied with a potential ranging from −0.4 to 0.1 V vs. SCE (−0.4, −0.3, −0.2, −0.1, 0.0, and 1.0 V *vs* SCE) for the forward scan and back to −0.4 V *vs* SCE (0.0, −0.1, −0.2, −0.3−0.4 V *vs* SCE) for the backward scan. Under each condition, the applied potential was held for 15 min before starting the XAS measurement to confirm the steady state. The white light was shone on the electrode during the *in situ* XAS experiment to investigate the effect of light illumination on the as-synthesized photoelectrode materials, as shown in Figure S1.

DFT Calculation Details. All calculations reported in this work were performed by VASP[20−22] based on the periodic plane-wave DFT. The interaction between ion cores and valence electrons was accounted by the projector-augmented wave[25] pseudopotentials. The exchange and correlation interactions between electrons were treated within the generalized gradient approximation[26] with the Perdew−Burke−Ernzerhof[27] parameterization. The additional van der Waals contributions were obtained through the semiempirical D2 method of Grimme (DFT-D2).[28] The effect of 3d electron correlation can be improved by considering on-site Coulomb (U) and exchange (J) interactions. On-site Hubbard term U − J values[29] of 5.7 and 1.5 eV[30] were applied for Co and Ag atoms, respectively. The cutoff energy for the expanded plane-wave basis set was set to 540 eV. The convergence thresholds for full geometry optimizations were set to 10^{-5} eV and 0.005 eV/Å for each electronic step and ionic step, respectively. The Brillouin zone integration was sampled via the Monkhorst−Pack[31] method with the 8 × 8 × 8 *k*-point mesh for bulk. The optimized lattice constants of the bulk unit cell are obtained as *c* = 4.594 Å for β-$Co(OH)_2$ and *c* = 7.09 Å for Ag-α-$Co(OH)_2$. This is reasonably in agreement with the experimentally obtained d-spacing values, 4.6 Å from the literature for β-$Co(OH)_2$ and 7.0 Å for ion-implanted α-$Co(OH)_2$.[2−6] The band structure calculations in Figure 3 indicates that the presence of Ag in the structure of α-$Co(OH)_2$ causes a decrease in the band gap..

ASSOCIATED CONTENT

Supporting Information

The Supporting Information is available free of charge at https://pubs.acs.org/doi/10.1021/acsomega.1c01908.

In situ electrochemical XAS experiment setup, additional results such as FE-SEM, HR-TEM coupled with EDS, XRD patterns, areal stored charge obtained from CVs, and *in situ* XAS (PDF)

AUTHOR INFORMATION

Corresponding Author

Montree Sawangphruk − *Centre of Excellence for Energy Storage Technology (CEST), Department of Chemical and Biomolecular Engineering, School of Energy Science and Engineering, Vidyasirimedhi Institute of Science and Technology, Rayong 21210, Thailand; Research Network of NANOTEC-VISTEC on Nanotechnology for Energy,*

https://doi.org/10.1021/acsomega.1c01908
ACS Omega 2021, 6, 20804−20811

Vidyasirimedhi Institute of Science and Technology, Rayong 21210, Thailand; orcid.org/0000-0003-2769-4172; Phone: 66(0)33-01-4251; Email: montree.s@vistec.ac.th; Fax: 66(0)33-01-4445

Authors

Montakan Suksomboon − *Centre of Excellence for Energy Storage Technology (CEST), Department of Chemical and Biomolecular Engineering, School of Energy Science and Engineering, Vidyasirimedhi Institute of Science and Technology, Rayong 21210, Thailand*

Ketsuda Kongsawatvoragul − *Centre of Excellence for Energy Storage Technology (CEST), Department of Chemical and Biomolecular Engineering, School of Energy Science and Engineering, Vidyasirimedhi Institute of Science and Technology, Rayong 21210, Thailand*

Salatan Duangdangchote − *Centre of Excellence for Energy Storage Technology (CEST), Department of Chemical and Biomolecular Engineering, School of Energy Science and Engineering, Vidyasirimedhi Institute of Science and Technology, Rayong 21210, Thailand*

Complete contact information is available at: https://pubs.acs.org/10.1021/acsomega.1c01908

Notes

The authors declare no competing financial interest.

■ ACKNOWLEDGMENTS

This work was financially supported by Thailand Research Fund and the Vidyasirimedhi Institute of Science and Technology (RSA6180031 and RTA6080005) as well as Energy Policy and Planning Office (EPPO), Ministry of Energy, Thailand. Support from the Frontier Research Centre at VISTEC and Synchrotron Light Research Institute (Public Organization), Beam 5.2, Thailand, for XANES is also acknowledged. This work has been partially supported by the NANOTEC, NSTDA, Ministry of Science and Technology, Thailand, through its program of Research Network NANOTEC. Support from IRPC Pub Co., Ltd., PTTEP Pub Co., Ltd., Taioil Pub Co., Ltd., PTTGC Pub Co., Ltd., GPSC Pub Co., Ltd., PTTOR Pub Co., Ltd., and PTT Pub Co., Ltd. is also acknowledged.

■ REFERENCES

(1) Pang, H.; Li, X.; Zhao, Q.; Xue, H.; Lai, W.-Y.; Hu, Z.; Huang, W. One-pot synthesis of heterogeneous Co_3O_4-nanocube/$Co(OH)_2$-nanosheet hybrids for high-performance flexible asymmetric all-solid-state supercapacitors. *Nano Energy* **2017**, *35*, 138−145.

(2) Ma, R.; Liu, Z.; Takada, K.; Fukuda, K.; Ebina, Y.; Bando, Y.; Sasaki, T. Tetrahedral Co(II) Coordination in α-Type Cobalt Hydroxide: Rietveld Refinement and X-ray Absorption Spectroscopy. *Inorg. Chem.* **2006**, *45*, 3964−3969.

(3) Kalasina, S.; Pattanasattayavong, P.; Suksomboon, M.; Phattharasupakun, N.; Wutthiprom, J.; Sawangphruk, M. A new concept of charging supercapacitors based on the photovoltaic effect. *Chem. Commun.* **2017**, *53*, 709−712.

(4) Neilson, J. R.; Schwenzer, B.; Seshadri, R.; Morse, D. E. Kinetic Control of Intralayer Cobalt Coordination in Layered Hydroxides: $Co_{1-0.5x}{}^{oct}Co_x{}^{tet}(OH)_2(Cl)_x(H_2O)_n$. *Inorg. Chem.* **2009**, *48*, 11017−11023.

(5) Liu, Z.; Ma, R.; Osada, M.; Takada, K.; Sasaki, T. Selective and Controlled Synthesis of α- and β-Cobalt Hydroxides in Highly Developed Hexagonal Platelets. *J. Am. Chem. Soc.* **2005**, *127*, 13869−13874.

(6) Rahbani, J.; Khashab, N. M.; Patra, D.; Al-Ghoul, M. Kinetics and mechanism of ionic intercalation/de-intercalation during the formation of α-cobalt hydroxide and its polymorphic transition to β-cobalt hydroxide: reaction−diffusion framework. *J. Mater. Chem.* **2012**, *22*, 16361−16369.

(7) Martinez, E. Y.; Zhu, K.; Li, C. W. Influence of the Defect Stability on n-Type Conductivity in Electron-Doped α- and β-$Co(OH)_2$ Nanosheets. *Inorg. Chem.* **2021**, *60*, 6950−6956.

(8) Oestreicher, V.; Hunt, D.; Torres-Cavanillas, R.; Abellán, G.; Scherlis, D. A.; Jobbágy, M. Halide-Mediated Modification of Magnetism and Electronic Structure of α-Co(II) Hydroxides: Synthesis, Characterization, and DFT+U Simulations. *Inorg. Chem.* **2019**, *58*, 9414−9424.

(9) Kalasina, S.; Kongsawatvoragul, K.; Phattharasupakun, N.; Phattharaphuti, P.; Sawangphruk, M. Cobalt oxysulphide/hydroxide nanosheets with dual properties based on electrochromism and a charge storage mechanism. *RSC Adv.* **2020**, *10*, 14154−14160.

(10) Kalasina, S.; Phattharasupakun, N.; Sawangphruk, M. A new energy conversion and storage device of cobalt oxide nanosheets. *J. Mater. Chem. A* **2018**, *6*, 36−40.

(11) Kalasina, S.; Kongsawatvoragul, K.; Phattharasupakun, N.; Sawangphruk, M. Thin-Film Photoelectrode of p-Type Ni-Doped Co3O4 Nanosheets for a Single Hybrid Energy Conversion and Storage Cell. *J. Electrochem. Soc.* **2019**, *166*, A2444−A2452.

(12) Kongsawatvoragul, K.; Kalasina, S.; Phattharasupakun, N.; Sawangphruk, M. A single energy conversion and storage cell of nickel-doped cobalt oxide under UV and visible light illumination. *Electrochim. Acta* **2019**, *328*, 135120.

(13) Kongsawatvoragul, K.; Chomkhuntod, P.; Sawangphruk, M. Solar-driven Energy Storage Enhancement of Nickel Hydroxide Nanomaterials. *Electrochim. Acta* **2021**, *388*, 138654.

(14) Tomon, C.; Sarawutanukul, S.; Duangdangchote, S.; Krittayavathananon, A.; Sawangphruk, M. Photoactive Zn−air batteries using spinel-type cobalt oxide as a bifunctional photocatalyst at the air cathode. *Chem. Commun.* **2019**, *55*, 5855−5858.

(15) Yu, J. M.; Lee, J.; Kim, Y. S.; Song, J.; Oh, J.; Lee, S. M.; Jeong, M.; Kim, Y.; Kwak, J. H.; Cho, S.; Yang, C.; Jang, J.-W. High-performance and stable photoelectrochemical water splitting cell with organic-photoactive-layer-based photoanode. *Nat. Commun.* **2020**, *11*, 5509.

(16) Nguyen, T.; Montemor, M. d. F. Metal Oxide and Hydroxide-Based Aqueous Supercapacitors: From Charge Storage Mechanisms and Functional Electrode Engineering to Need-Tailored Devices. *Adv. Sci.* **2019**, *6*, 1801797.

(17) Fu, L.; Qu, Q.; Holze, R.; Kondratiev, V. V.; Wu, Y. Composites of metal oxides and intrinsically conducting polymers as supercapacitor electrode materials: the best of both worlds? *J. Mater. Chem. A* **2019**, *7*, 14937−14970.

(18) Guan, M.; Wang, Q.; Zhang, X.; Bao, J.; Gong, X.; Liu, Y. Two-Dimensional Transition Metal Oxide and Hydroxide-Based Hierarchical Architectures for Advanced Supercapacitor Materials. *Front. Chem.* **2020**, *8*, 390.

(19) Suksomboon, M.; Khuntilo, J.; Kalasina, S.; Suktha, P.; Limtrakul, J.; Sawangphruk, M. High-performance energy storage of Ag-doped $Co(OH)_2$-coated graphene paper: In situ electrochemical X-ray absorption spectroscopy. *Electrochim. Acta* **2017**, *252*, 91−100.

(20) Kresse, G.; Hafner, J. Ab initio molecular dynamics for liquid metals. *Phys. Rev. B: Condens. Matter Mater. Phys.* **1993**, *47*, 558−561.

(21) Kresse, G.; Furthmüller, J. Efficiency of ab-initio total energy calculations for metals and semiconductors using a plane-wave basis set. *Comput. Mater. Sci.* **1996**, *6*, 15−50.

(22) Kresse, G.; Furthmüller, J. Efficient iterative schemes for ab initio total-energy calculations using a plane-wave basis set. *Phys. Rev. B: Condens. Matter Mater. Phys.* **1996**, *54*, 11169−11186.

(23) Tan, H.; Santbergen, R.; Smets, A. H. M.; Zeman, M. Plasmonic Light Trapping in Thin-film Silicon Solar Cells with Improved Self-Assembled Silver Nanoparticles. *Nano Lett.* **2012**, *12*, 4070−4076.

(24) Iamprasertkun, P.; Krittayavathananon, A.; Seubsai, A.; Chanlek, N.; Kidkhunthod, P.; Sangthong, W.; Maensiri, S.; Yimnirun, R.; Nilmoung, S.; Pannopard, P.; Ittisanronnachai, S.; Kongpatpanich, K.; Limtrakul, J.; Sawangphruk, M. Charge storage mechanisms of manganese oxide nanosheets and N-doped reduced graphene oxide aerogel for high-performance asymmetric supercapacitors. *Sci. Rep.* **2016**, *6*, 37560.
(25) Kresse, G.; Joubert, D. From ultrasoft pseudopotentials to the projector augmented-wave method. *Phys. Rev. B: Condens. Matter Mater. Phys.* **1999**, *59*, 1758−1775.
(26) Perdew, J. P.; Burke, K.; Ernzerhof, M. Generalized Gradient Approximation Made Simple. *Phys. Rev. Lett.* **1996**, *77*, 3865−3868.
(27) Perdew, J. P.; Ernzerhof, M.; Burke, K. Rationale for mixing exact exchange with density functional approximations. *J. Chem. Phys.* **1996**, *105*, 9982−9985.
(28) Stefan, G. Semiempirical GGA-type density functional constructed with a long-range dispersion correction. *J. Comput. Chem.* **2006**, *27*, 1787−1799.
(29) Anisimov, V. I.; Zaanen, J.; Andersen, O. K. Band theory and Mott insulators: Hubbard U instead of Stoner I. *Phys. Rev. B: Condens. Matter Mater. Phys.* **1991**, *44*, 943−954.
(30) Mueller, T.; Hautier, G.; Jain, A.; Ceder, G. Evaluation of Tavorite-Structured Cathode Materials for Lithium-Ion Batteries Using High-Throughput Computing. *Chem. Mater.* **2011**, *23*, 3854−3862.
(31) Monkhorst, H. J.; Pack, J. D. Special points for Brillouin-zone integrations. *Phys. Rev. B: Condens. Matter Mater. Phys.* **1976**, *13*, 5188−5192.

https://doi.org/10.1021/acsomega.1c01908
ACS Omega 2021, 6, 20804−20811